

# Verification of an Electrochemical Model for Aqueous Corrosion of Mild Steel for H<sub>2</sub>S Partial Pressures up to 0.1 MPa

Saba Navabzadeh Esmaeely,<sup>‡,\*</sup> Bruce Brown,<sup>\*</sup> and Srdjan Nešić<sup>\*</sup>

## ABSTRACT

Hydrogen sulfide (H<sub>2</sub>S) corrosion of mild steel is a serious concern in the oil and gas industry. However, H<sub>2</sub>S corrosion mechanisms, specifically at high partial pressures of H<sub>2</sub>S (pH<sub>2</sub>S), have not been extensively studied because of experimental difficulties and associated safety issues. The current study was conducted under well-controlled conditions at pH<sub>2</sub>S of 0.05 MPa and 0.096 MPa. The pH range used was from pH 3.0 to pH 5.0, at temperatures of 30°C and 80°C, and with rotating cylinder speeds of 100 rpm and 1,000 rpm. Short-term exposures, lasting between 1.0 h and 1.5 h, were used to avoid formation of any protective iron sulfide layers. The experimental results were compared with a recent mechanistic model of sour corrosion developed by Zheng, et al. (2014). This model was based on corrosion experiments conducted at low pH<sub>2</sub>S (0.0001 kPa to 10 kPa) and is applicable only to conditions where protective iron sulfide layers do not form. The validity of the model at higher pH<sub>2</sub>S was examined, as it was uncertain if the mechanisms identified at lower pH<sub>2</sub>S were still valid. The comparison with the experimental results obtained in the present study indicated a good agreement between the model and the measurements. This confirmed that the physicochemical processes underlying H<sub>2</sub>S corrosion in the absence of protective iron sulfides are very similar across a wide range of H<sub>2</sub>S aqueous concentrations. It also demonstrated that the mechanistic corrosion model was reasonable when extrapolating from low to high pH<sub>2</sub>S.

**KEY WORDS:** corrosion rate, hydrogen evolution, hydrogen sulfide, pH changes and effects, potentiodynamic

## INTRODUCTION

The role of hydrogen sulfide (H<sub>2</sub>S) on aqueous mild steel corrosion has been one of the concerns of corrosion researchers since 1940.<sup>1-13</sup> Ewing<sup>14</sup> and Sardisco, et al.,<sup>15</sup> were among the first scholars to initiate controlled H<sub>2</sub>S corrosion experimentation, which was later continued by other researchers.<sup>13,16-20</sup> The focus of much of the H<sub>2</sub>S-related studies in the past was on iron sulfide formation and the resulting effect on corrosion.<sup>3,21-23</sup> The vast majority of the available research results come from experiments conducted at lower H<sub>2</sub>S partial pressures (pH<sub>2</sub>S < 10<sup>-2</sup> MPa). Over the past few decades, a significant number of new oil and gas fields are sour, ranging from a few ppm up to 15 mol% to 20 mol% H<sub>2</sub>S (e.g., the Kashagan Field<sup>24</sup>). This indicates a growing need for better understanding of H<sub>2</sub>S corrosion mechanisms and more effective prediction tools, particularly at higher pH<sub>2</sub>S.

Uncertainties related to modeling of H<sub>2</sub>S corrosion are particularly pronounced at higher pH<sub>2</sub>S. Under those conditions, limited results are available. Therefore, most of the models developed so far are based on lower pH<sub>2</sub>S. Despite the progress in understanding of H<sub>2</sub>S corrosion,<sup>1-35</sup> there is still a lack of systematic studies where the parameter space has been explored in an organized way. Again, the problem is even more pronounced at higher pH<sub>2</sub>S, where the challenges associated with conducting experiments are much bigger. Corrosion data that have been reported under these conditions in the open literature are very few, with widely scattered operating conditions.

Submitted for publication: June 16, 2016. Revised and accepted: August 31, 2016. Preprint available online: August 31, 2016, <http://dx.doi.org/10.5006/2172>.

<sup>‡</sup> Corresponding author. E-mail: [sn294410@ohio.edu](mailto:sn294410@ohio.edu).

<sup>\*</sup> Institute for Corrosion and Multiphase Technology, Department of Chemical and Biomolecular Engineering, Ohio University, OH 45701.

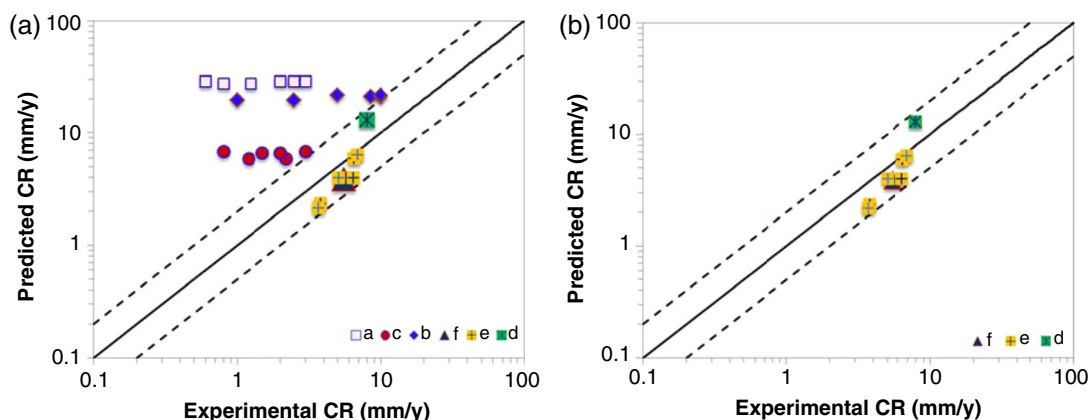


**FIGURE 1.** Parity plot of the predicted data using Zheng's model when there is no iron sulfide layer vs. experimental data at higher  $p\text{H}_2\text{S}$ .<sup>24,27-29</sup>

There has been substantial progress in understanding and modeling of  $\text{H}_2\text{S}$ -related corrosion since the late 1990's. In 2009, Sun and Nešić<sup>19</sup> proposed a mechanistic  $\text{H}_2\text{S}$  model that accounted for iron sulfide layer formation. It assumed that the corrosion rate was always under mass transfer control with the iron sulfide layer being dominant, and it did not take into account the kinetics of electrochemical reactions. While this has been proven to be an overly restrictive assumption, the work conducted by Sun and Nešić<sup>19</sup> provided a foundation for further investigation and modeling of  $\text{H}_2\text{S}$  corrosion mechanisms in a more systematic way.

In 2014 and 2015, Zheng, et al.,<sup>20,25</sup> developed a mechanistic model of pure  $\text{H}_2\text{S}$  and mixed  $\text{CO}_2/\text{H}_2\text{S}$  corrosion of mild steel that considered both the electrochemical and mass transfer controlled reactions. This model calculates the corrosion rate in the absence of iron sulfide layers. The authors were able to demonstrate that when mild steel was exposed to aqueous  $\text{H}_2\text{S}$ , the direct reduction of  $\text{H}_2\text{S}$  occurs on the steel surface as an additional hydrogen evolution reaction. The model was validated with experimental data from corrosion experiments conducted in an aqueous solution sparged with  $\text{H}_2\text{S}$  at partial pressures from  $10^{-7}$  MPa to  $10^{-2}$  MPa.<sup>20,25</sup>

The focus of the current study is on the higher  $p\text{H}_2\text{S}$  and the corrosion mechanisms of mild steel at those conditions. One of the key hypotheses is that the mechanistic model,<sup>20,25</sup> based on low  $p\text{H}_2\text{S}$  data, will perform at higher  $p\text{H}_2\text{S}$ . To prove this, one needs reliable experimental data at higher  $p\text{H}_2\text{S}$ ; thus, a number of experimental studies were found in the available open literature. The choice of literature data was made according the following criteria: the corrosion study had to be comprehensively reported, including a proper description of the experimental setup, procedures, and data analysis. For example, studies that failed to describe the water chemistry or some other key experimental parameters were not

considered, even if the corrosion results were reported. Furthermore, only the experimental data that were obtained in short exposures, prior to formation of protective iron sulfide corrosion product layers, were considered in order to compare with the model.<sup>20,25</sup>

The results of this exercise are given in Figure 1(a), which shows parity plots where all of the selected experimental corrosion rate data from the open literature at high  $p\text{H}_2\text{S}$  are plotted vs. the predictions made by the model. The solid lines in Figure 1 represent a perfect agreement, while the dashed lines represent a factor of two difference between the measured and predicted values. The different colors of the symbols indicate data from different experimental conditions and/or different studies.

In this comparison, it appears that the model overpredicts the majority of the measured corrosion rates. However, before drawing any conclusions about the performance of the model, it is essential to reconfirm that the experimental data were consistent and suitable for the present exercise. All of the outliers, shown on the parity plot in Figure 1(a), were generated in a single experimental study by Omar, et al.<sup>24</sup> The authors presented time series from long-term experiments; hence, only the data points reported at time "zero" were used here. After analyzing the data of Omar, et al.,<sup>24</sup> it seems likely that an iron sulfide layer had formed on the specimens' surface prior to that first reported corrosion rate measurement. The challenge the authors faced was in the fast kinetics of iron sulfide formation reactions in high  $\text{H}_2\text{S}$ -containing environments.<sup>26</sup> They reported lower corrosion rates for higher  $p\text{H}_2\text{S}$  and  $p\text{CO}_2$  (as listed in Table 1), which can only happen if protective iron carbonate and/or iron sulfide layers formed. Consequently, these data points were eliminated from the present study.

The reduced number of data points collected at high  $p\text{H}_2\text{S}$  now appears to be within a factor of two of the model predictions, as shown in Figure 1(b). The

**TABLE 1**  
Summary of Results

Test Conditions	Reported Corrosion Rate (mm/y)	Predicted Corrosion Rate (mm/y)	Reference	Legend
1 MPa H <sub>2</sub> S; 0.33 MPa CO <sub>2</sub> ; pH 3.1; 1, 3, and 5 m/s; 80°C	1 to 10	19 to 21	Omar, et al. <sup>24</sup>	b
1 MPa H <sub>2</sub> S; 0.33 MPa CO <sub>2</sub> ; pH 3.2; 1, 3, and 5 m/s; 25°C	2 to 3	5 to 6	Omar, et al. <sup>24</sup>	c
3 MPa H <sub>2</sub> S; 1 MPa CO <sub>2</sub> ; pH 3.0; 1, 3, and 5 m/s; 80°C	0.8 to 2	27 to 28	Omar, et al. <sup>24</sup>	a
0.14 MPa H <sub>2</sub> S; 0.06 MPa CO <sub>2</sub> ; pH 4.5; 1 m/s; 60°C	5.5	3.8	Kvarekval and Dugstad <sup>27</sup>	d
0.088 MPa H <sub>2</sub> S; pH 4.2; 50°C	3.7	2.4	Abayarathna <sup>28</sup>	e
0.069 MPa H <sub>2</sub> S; pH 4.2; 70°C	5.1	3.9	Abayarathna <sup>28</sup>	e
0.03 MPa H <sub>2</sub> S; pH 4.2; 90°C	6.9	6.3	Abayarathna <sup>28</sup>	e
0.044 MPa H <sub>2</sub> S; 0.044 MPa CO <sub>2</sub> ; pH 4.2; 50°C	3.8	2.3	Abayarathna <sup>28</sup>	e
0.034 MPa H <sub>2</sub> S; 0.034 MPa CO <sub>2</sub> ; pH 4.2; 70°C	6.4	3.6	Abayarathna <sup>28</sup>	e
0.015 MPa H <sub>2</sub> S; 0.015 MPa CO <sub>2</sub> ; pH 4.2; 90°C	6.5	5.8	Abayarathna <sup>28</sup>	e
1.6 MPa H <sub>2</sub> S; 90°C	8	12.8	Liu, et al. <sup>29</sup>	f

remaining eight data points came from three different high pH<sub>2</sub>S corrosion studies, with widely different conditions and with no additional information on underlying corrosion mechanisms. This illustrates that there is a clear lack of reliable, systematically collected, coherent corrosion data from high pH<sub>2</sub>S experiments, based on sound electrochemical measurements. Therefore, the present study is meant to fill

this gap, and provide a solid base for verification of mechanisms and models for mild steel corrosion in high pH<sub>2</sub>S environments.

## EXPERIMENTAL METHODS AND SETUP

Experiments were conducted in a glass cell (see Figure 2), which was filled with 2 L of deionized water

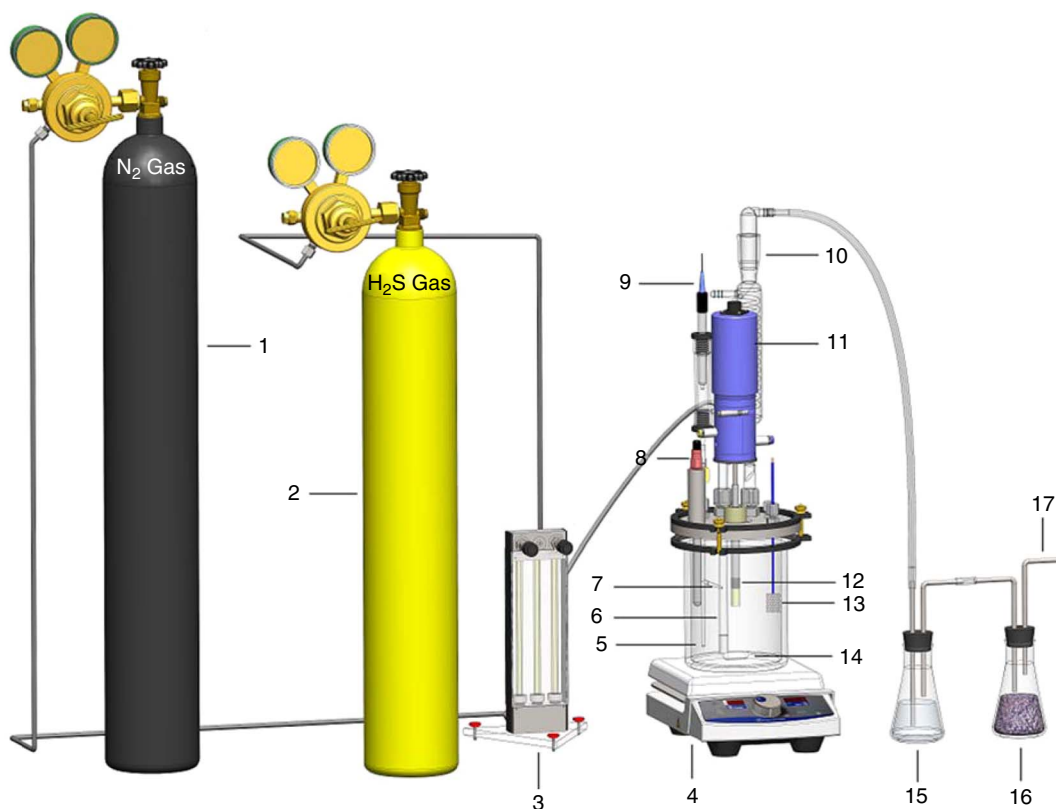


**FIGURE 2.** Experimental setup with: 1. N<sub>2</sub> gas cylinder, 2. H<sub>2</sub>S gas cylinder, 3. Rotameter, 4. Hot plate, 5. Temperature probe, 6. Gas inlet, 7. Luggin capillary, 8. pH-electrode, 9. Reference electrode, 10. Condenser, 11. Rotating cylinder shaft, 12. Working electrode, 13. Platinum counter electrode, 14. Stir bar (0.5 in [1.72 cm] in length), 15. Sodium hydroxide solution, 16. Carbon scrubber, 17. Gas outlet. Image is courtesy of Cody Shafer.

and 60.6 g NaCl to obtain a 3.0 wt% solution. The solution was deoxygenated by purging with N<sub>2</sub> for 3 h and was then saturated with H<sub>2</sub>S by continuously purging the solution with H<sub>2</sub>S gas throughout the remainder of the experiment. The gas outlet was scrubbed using a 5 M solution of sodium hydroxide (NaOH) and a series of dry carbon scrubbers. The solution pH was adjusted to the desired value by addition of a deoxygenated hydrochloric acid (HCl) or a NaOH solution. It was deemed that equilibrium in the solution was reached after approximately 1 h after the introduction of H<sub>2</sub>S gas into the glass cell.

A cylindrical API X65 steel specimen was sequentially polished with 150, 400, and 600 grit sandpaper, rinsed with isopropyl alcohol in an ultrasonic bath, and air dried. It was then mounted onto the rotating cylinder (RCE) rotator and inserted into the glass cell for electrochemical measurements. The rotator was set to the desired rotational speed and the corrosion measurements were initiated.

Electrochemical measurements were conducted using a three-electrode setup with a mild steel RCE as the working electrode (WE). A platinum mesh plate was used as the counter electrode (CE). An external saturated silver/silver chloride (Ag/AgCl) reference electrode (RE) was connected using a KCl salt bridge via a Luggin capillary. Open-circuit potential (OCP) measurements were done first to ensure that a reasonably stable state was reached, where the OCP drift was less than 1 mV per min and the magnitude of the OCP fluctuation was less than 1 mV (this occurred typically within the first 5 min). The OCP measurements were immediately followed by electrochemical impedance spectroscopy (EIS) in order to determine the solution resistance (IR drop). Then, the linear polarization resistance (LPR) measurements were conducted in order to estimate the polarization resistance ( $R_p$ ) and the corrosion rate. Finally, potentiodynamic measurements were conducted by first sweeping the potential from the OCP in the cathodic direction. After the OCP stabilized (usually within 10 min), the anodic potential sweep was performed.

During the LPR measurements, the WE was polarized  $\pm 5$  mV from the OCP in order to determine the ( $R_p$ ), using a scan rate of 0.125 mV/s. The measured  $R_p$  was corrected for the solution resistance that was obtained from the high-frequency portion of the EIS spectrum (frequency range around 5 kHz). The linear polarization constant,  $B = 23$  mV/decade, was used in the current work based on comparison of LPR measurements with weight loss.<sup>20</sup> Potentiodynamic sweeps were conducted at a rate of 5 mV/s. While this is generally considered a very fast sweep rate, where transient effects could interfere, it was an imperative to complete the measurements in the shortest possible

**TABLE 2**  
Experiment Matrix

Parameters	Conditions
Total Pressure	0.1 MPa
Temperature	30°C and 80°C
Solution	3 wt% NaCl
Test Condition	1,000 rpm, 100 rpm
Material	X65
Methods	LPR, EIS, and Potentiodynamic Sweep
pH <sub>2</sub> S in the Gas Phase	0, 0.053, and 0.096 MPa
pH Value	2.0, 3.0, 4.0, and 5.0 ( $\pm 0.1$ )

time, in order to avoid formation of protective iron sulfide layers. Also, the fast sweep rate minimized the atomic hydrogen diffusion into the steel, which allowed the surface to recover to the OCP in a shorter period. In order to confirm that the fast sweep rate was acceptable, the potentiodynamic sweeps obtained at a low pH and low temperature (where formation of iron sulfide was slower) were compared by using sweep rates of 1 mV/s and 5 mV/s, with no substantial difference seen. Each potentiodynamic sweep was corrected for the ohmic drop resulting from solution resistance. The experiments were conducted at three different pH, and two different velocities and temperatures, as summarized in Table 2.

## MODELING

The electrochemical corrosion model used in the current study was previously described by Zheng, et al.<sup>20</sup> Based on details presented in that publication and the references within, the model was reconstructed by using MATLAB<sup>†</sup>—a popular numerical computing environment. In the text presented next, the key elements of the model are given, in order to facilitate the following of the arguments and analysis. The model is based on a standard mathematical description of electrochemical, chemical, and mass transfer processes, underlying the theory of aqueous H<sub>2</sub>S corrosion of mild steel.

### Cathodic Reactions

In H<sub>2</sub>S-containing environments, three main cathodic reactions are considered: H<sup>+</sup> reduction, H<sub>2</sub>S reduction, and H<sub>2</sub>O reduction.

*H<sup>+</sup> Reduction* — The H<sup>+</sup> reduction is the dominant cathodic reaction in acidic solutions:



Because of fast kinetics, it is often limited by H<sup>+</sup> diffusion to the steel surface. The H<sup>+</sup> reduction current density  $i_{c(\text{H}^+)}$  is calculated using the equations given in Table 3, and considers both charge transfer and mass transfer limiting currents.<sup>30</sup> The charge transfer current density is calculated by the Tafel equation. The

<sup>†</sup> Trade name.

TABLE 3

Calculation of the H<sup>+</sup> Reduction Current Density<sup>(A)</sup>

$\frac{1}{i_{c(H^+)}} = \frac{1}{i_{a(H^+)}} + \frac{1}{i_{d(H^+)}}$	(2)
$i_{\alpha(H^+)} = i_{(H^+)}^0 10^{(-E_{corr} - E_{rev(H^+)})/b_{c(H^+)}}$	(3)
$i_{(H^+)}^0 = i_{ref}^0 \left( \frac{C_{H^+}}{C_{H^+ref}} \right)^{0.5} e^{-\frac{\Delta H}{R} \left( \frac{1}{T} - \frac{1}{T_{ref}} \right)}$	(4)
$i_{ref}^0 = 0.03 \text{ A/m}^2, C_{H^+ref} = 1 \times 10^{-4} \text{ mol/L}, \Delta H = 30 \text{ kJ/mol}^{32}$	
$E_{rev(H^+)} = -\frac{2.303RT}{F} \text{pH} - \frac{2.303RT}{2F} \log P_{H_2}$	(5)
$b_c = \frac{2.0303RT}{\alpha_c F}, \alpha_c = 0.5, \text{ and } b_c = 0.5 \text{ V/decade}^{33}$	(6)
$i_{(H^+)}^d = k_{m(H^+)} F C_{H^+}$	(7)
$Sh = \frac{k_{m(H^+)} d_{RCE}}{D_{H^+}} = 0.0791 \text{ Re}^{0.7} \text{ Sc}^{0.356}$	(8)
$D_{H^+} = D_{refH^+} \frac{T_K}{T_{ref}} \frac{\mu_{ref}}{\mu}$	(9)
$\mu = \mu_{ref} 10^{\frac{1.3272(20-T_K) - 0.001053(20-T_K)^2}{T_K + 105}}$	(10)

(A) The nomenclature is defined in a separate section at the end of the paper.

mass transfer current density is calculated with the aid of a mass transfer coefficient, utilizing the empirical correlation between the Sherwood number and the Reynolds/Schmidt numbers for the flow geometry of interest (in the present case an RCE).<sup>31</sup>

**H<sub>2</sub>S Direct Reduction** — Aqueous H<sub>2</sub>S is a weak acid and is the main source of H<sup>+</sup> ions, obtained by partial dissociation:

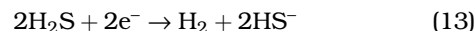


However, Zheng, et al.,<sup>20,25</sup> provided conclusive evidence that the main contribution to the corrosion process is the direct reduction of aqueous H<sub>2</sub>S on the steel surface.

TABLE 4

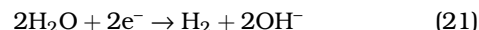
Calculation of H<sub>2</sub>S Reduction Current Density

$\frac{1}{i_{c(H_2S)}} = \frac{1}{i_{a(H_2S)}} + \frac{1}{i_{d(H_2S)}}$	(14)
$i_{\alpha(H_2S)} = i_{(H_2S)}^0 10^{(-E_{corr} - E_{rev(H_2S)})/b_{c(H_2S)}}$	(15) <sup>20</sup>
$i_{(H_2S)}^0 = i_{ref}^0 \left( \frac{C_{H_2S}}{C_{H_2Sref}} \right)^{0.5} \left( \frac{C_{H^+}}{C_{H^+ref}} \right)^{-0.5} e^{-\frac{\Delta H}{R} \left( \frac{1}{T} - \frac{1}{T_{ref}} \right)}$	(16)
$i_{ref}^0 = 0.00015 \text{ A/m}^2, C_{H_2Sref} = 1 \times 10^{-4} \text{ mol/L},$	
$C_{H^+ref} = 1 \times 10^{-4} \text{ mol/L}, \Delta H = 60 \text{ kJ/mol}$	
$i_{(H_2S)}^d = k_{m(H_2S)} F C_{H_2S}$	(17)
$D_{H_2S} = D_{refH_2S} \frac{T_K}{T_{ref}} \frac{\mu_{ref}}{\mu}$	(18)
$C_{H_2S} = K_{sol(H_2S)} P_{H_2S}$	(19)
$K_{sol(H_2S)} = 10^{(634.27 + 0.2709T_K - 0.11132 \times 10^{-3} T_K^2 - \frac{16719}{T_K} - 261.9 \log T_K)}$	(20) <sup>34</sup>



This reaction can be either under charge transfer control or limited by mass transfer. The overall current density for direct reduction of aqueous H<sub>2</sub>S on the steel surface can be calculated in a similar way as was done for H<sup>+</sup> reduction, shown in Table 4.<sup>20</sup>

**H<sub>2</sub>O Reduction** — In acidic aqueous solutions containing H<sub>2</sub>S, direct water reduction is rarely significant; however, it was included in the model in order to enable a better comparison with the potentiodynamic sweeps, as shown below.



There is no mass transfer limitation for the water reduction reaction; thus, it was assumed that it is always under charge transfer control (see Table 5).

TABLE 5

Calculation of H<sub>2</sub>O Reduction Current Density

$i_{\alpha(H_2O)} = i_{(H_2O)}^0 10^{(-E_{corr} - E_{rev(H_2O)})/b_{c(H_2O)}}$	(22)
$i_{(H_2O)}^0 = i_{ref}^0 \left( \frac{C_{H_2O}}{C_{H_2Oref}} \right)^{-0.1} \left( \frac{C_{H^+}}{C_{H^+ref}} \right)^{-0.5} e^{-\frac{\Delta H}{R} \left( \frac{1}{T} - \frac{1}{T_{ref}} \right)}$	(23) <sup>20</sup>
$i_{ref}^0 = 2 \times 10^{-5} \text{ A/m}^2, C_{H_2Oref} = 1 \times 10^{-4} \text{ mol/L},$	
$C_{H^+ref} = 1 \times 10^{-4} \text{ mol/L}, \Delta H = 30 \text{ kJ/mol}^{35}$	

### Anodic Dissolution of Iron

In the presence of HS<sup>-</sup> in H<sub>2</sub>S aqueous solutions, the iron dissolution process follows a similar mechanism as originally proposed by Bockris, et al.,<sup>33</sup> for strong acids, and introduced by Ma, et al.:<sup>36</sup>

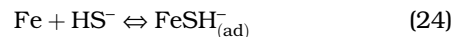
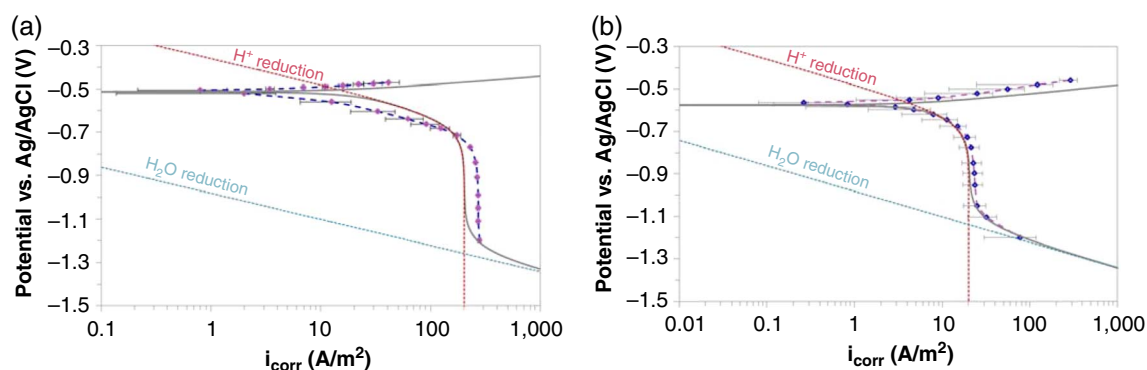


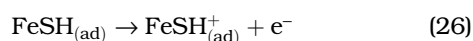
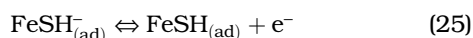
TABLE 6

Calculation of Current Density for Iron Dissolution

$i_{\alpha,Fe} = i_{(Fe)}^0 10^{(-E_{corr} - E_{rev(Fe)})/b_a}$	(27)
$b_c = 40 \text{ mV/decade}^{33}$	
$i_{(Fe)}^0 = i_{ref}^0 \theta_{HS^-} e^{-\frac{\Delta H}{R} \left( \frac{1}{T} - \frac{1}{T_{ref}} \right)}$	(28)
$i_{ref}^0 = 0.33 \text{ A/m}^2, \Delta H = 37.5 \text{ kJ/mol}^{20}$	
$\theta_{HS^-} = \frac{K_2 C_{HS^-}}{1 + K_2 C_{HS^-}}$	(29)
$K_2 = 3.5 \times 10^{620}$	
$C_{HS^-} = \frac{K_{H_2S} C_{H_2S}}{C_{H^+}}$	(30)
$K_{(H_2S)} = 10^{(782.43945 + 0.361261 T_K - 1.6722 \times 10^{-4} T_K^2 - \frac{20566.7315}{T_K} - 142.741722 \ln T_K)}$	(31) <sup>37</sup>



**FIGURE 3.** Potentiodynamic sweeps on mild steel in  $N_2$  purged solutions, 1 wt% NaCl, 30°C, and 1,000 rpm RCE, scan rate 5 mV/S: (a) pH 2.0 (2 repeats) and (b) pH 3.0 (6 repeats).



It is noteworthy that the current model does not take into account the H adsorption/absorption on the steel surface. It was assumed that iron dissolution was always under charge transfer control, with the anodic current density calculated using a Tafel equation as shown in Table 6.

### Calculation Procedure

The model requires the temperature, pH,  $p_{H_2S}$ , RCE diameter, and rotational velocity as the inputs, then it calculates the corrosion (open-circuit) potential by solving the charge balance equation:

$$i_{\text{Fe}} = i_{\text{H}^+} + i_{\text{H}_2\text{S}} + i_{\text{H}_2\text{O}} \quad (32)$$

To calculate the corrosion current density, the calculated corrosion potential is substituted into the expression for the anodic current density, shown in Table 6. The conversion from corrosion current density in  $A/m^2$  into the corrosion rate in mm/y was done using the Faraday's law:

$$\text{CR} = \frac{i_{\text{corr}} M_{\text{Fe}}}{2F\rho} (3,600 \times 24 \times 365) \quad (33)$$

In order for the model to generate potentiodynamic sweeps needed for a comparison with the experimental data, the potential was varied across the whole measured range and the absolute value of the net current (total cathodic minus total anodic) is calculated as:

$$i = i_{\text{H}^+} + i_{\text{H}_2\text{S}} + i_{\text{H}_2\text{O}} - i_{\text{Fe}} \quad (34)$$

## RESULTS AND DISCUSSION

To establish a baseline, the model calculations were first compared to potentiodynamic sweep data obtained in  $N_2$  saturated aqueous solutions at pH 2.0 and pH 3.0; the data were collected at room temperature in the absence of  $H_2S$ . The experimental repeatability and accuracy of the electrochemical measurements were quantified by repeating the experiments multiple times, as shown in Figure 3. There, the points represent the average value of the current obtained in different repeats and the error bars denote the maximum and minimum values, all taken at exactly the same potential.

Figure 3(a) shows that for pH 2.0, the experimentally measured current densities deviated from the model predictions by approximately 50% in the charge transfer region and about 25% in the limiting current region. The deviation seen in the limiting currents is statistically significant and possibly stems from excessive evolution of hydrogen gas bubbles, which altered the otherwise well-controlled mass transfer conditions in the vicinity of the electrode surface<sup>12</sup> at high current densities. The apparently large discrepancy seen in the charge transfer region of the potentiodynamic sweeps is not as significant, as the difference between calculated values and the averages of the measured values is of the same order of magnitude as the variation within the measured values themselves. In addition, it should be pointed out that the model was not developed to accurately predict in such low pH conditions, and there may be some physicochemical processes that are not captured well for the case of steel corrosion in strong acids. However, this is not a big concern as pH 2.0 lays outside the typical pH range seen in most  $H_2S$  dominated conditions.

The situation is markedly better at pH 3.0, as shown in Figure 3(b), where a very good agreement between the model and the measured data is seen, particularly for the cathodic reaction. These two sets of

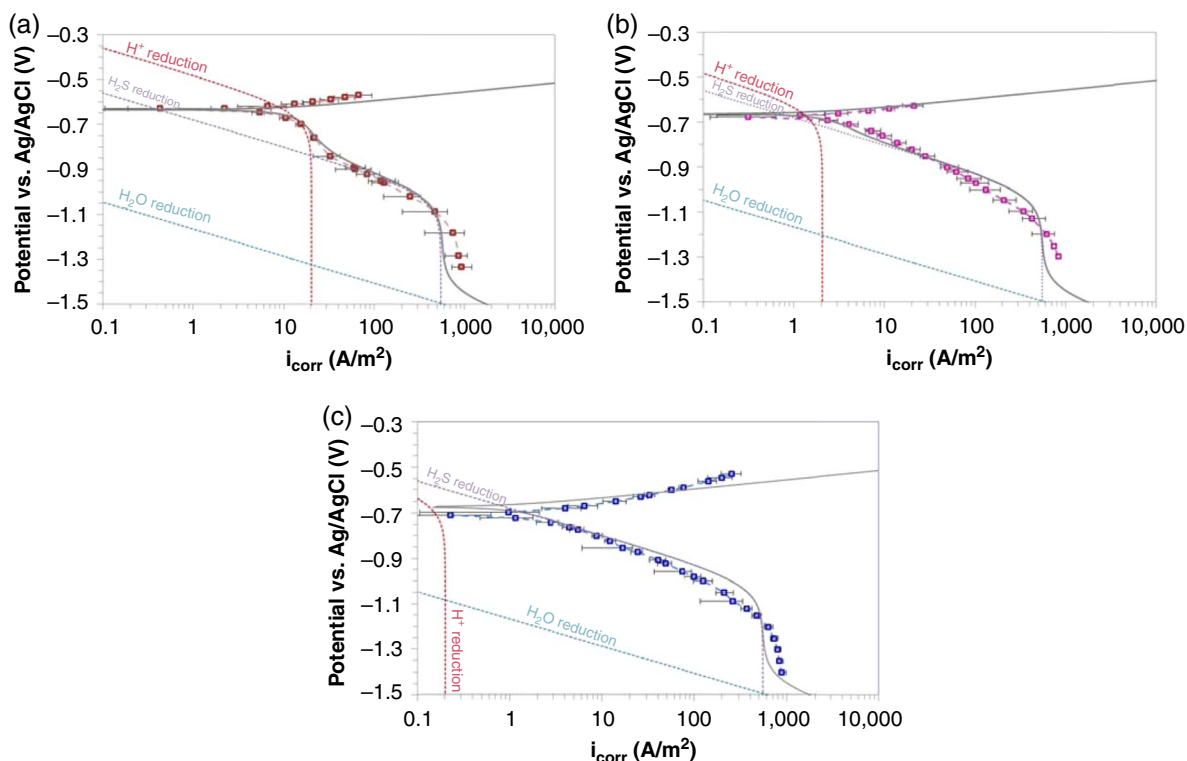


**FIGURE 4.** Potentiodynamic sweeps on mild steel in  $H_2S$  saturated solution with 0.096 MPa  $H_2S$  (960,000 ppm) in the gas phase, 3 wt% NaCl, 30°C, and 1,000 rpm RCE, scan rate 5 mV/S: (a) pH 3.0 (5 repeats), (b) pH 4.0 (4 repeats), and (c) pH 5.0 (6 repeats).

results obtained in the absence of  $H_2S$  confirm that both the model performance and the experimental procedures/techniques were at an acceptable level, providing a good foundation for the next step—comparison of the model with the data obtained in  $H_2S$  saturated conditions.

If the focus is now turned to  $H_2S$  saturated solution, the effect of pH is shown in Figure 4. In Figure 4(a), the measured data points show an average obtained from five repeats, conducted at the pH 3.0. There is a very good agreement between the measured data and the calculated ones, particularly at the lower current densities ( $<10 A/m^2$ ). The deviation in the limiting current at very high current densities ( $>500 A/m^2$ ) was probably a result of excessive formation of hydrogen gas bubbles at the electrode surface. The existence of the so-called “double wave” comes from the two independent cathodic reactions and their limiting currents.<sup>20,38</sup>

Similar results were obtained at pH 4.0, see Figure 4(b), which shows the averages of the data collected from four repeated experiments. Data from the experiments conducted at pH 5.0 are presented in Figure 4(c), which shows the averages from experiments repeated six times. It is clear that at the higher pH values, the reduction of  $H_2S$  dominates the rate of the cathodic reaction, as a result of a lower rate of  $H^+$

reduction because of a lower concentration of  $H^+$  ions. There seems to be a slight deviation between the measured and calculated Tafel slope for  $H_2S$  reduction, which is difficult to explain. It may be the result of a measurements error obtained at the higher current densities ( $>10 A/m^2$ ) or a result of the inaccuracy of the model at these conditions. Either way, this is not expected to affect the corrosion rate calculation in a

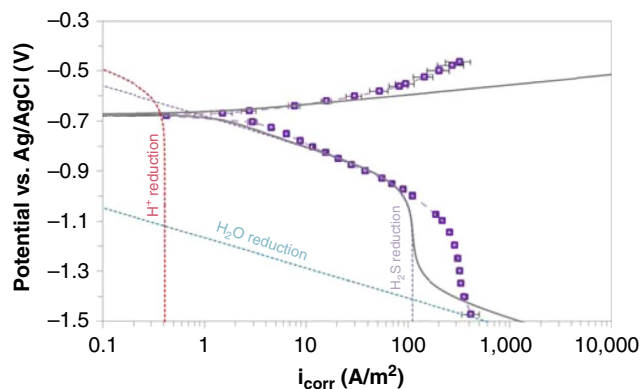


**FIGURE 5.** Potentiodynamic sweeps on mild steel in  $H_2S$  saturated solution with 0.096 MPa  $H_2S$  (960,000 ppm) in the gas phase, pH 4.0, 3 wt% NaCl, 30°C, and 1,000 rpm RCE, scan rate 5 mV/S, 2 repeats.

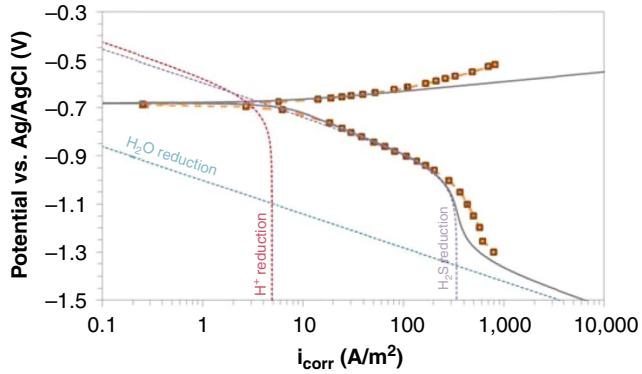


**FIGURE 6.** Potentiodynamic sweeps on carbon steel in  $H_2S$  saturated solution with  $0.053$  MPa  $H_2S$  (530,000 ppm) in the gas phase, pH 4.0, 3 wt% NaCl,  $80^\circ C$ , and 1,000 rpm RCE; scan rate 5 mV/S, 2 repeats.

significant way, as the corrosion current densities are typically below  $10$  A/m<sup>2</sup>.

For data collected at pH 5.0, presented in Figure 4(c), there is an approximately 50 mV deviation between the calculated and the measured OCP. This problem is most likely associated with the modeling of the anodic (iron dissolution) current. To confirm this and eliminate any possible experimental error associated with iron sulfide layer formation during the cathodic sweeps (which were conducted first), a new experiment was organized where the anodic sweep

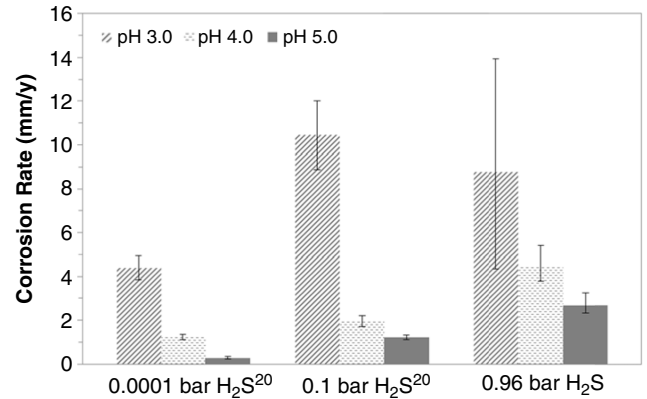


**FIGURE 8.** LPR uniform corrosion rate of X65 in a bulk solution with  $10^{-5}$  MPa  $H_2S$  (100 ppm),<sup>20</sup>  $10^{-2}$  MPa  $H_2S$  (100,000 ppm),<sup>20</sup> and  $0.096$  MPa  $H_2S$  (960,000 ppm), at  $30^\circ C$ , 1,000 rpm, 3 wt% NaCl, and  $B = 23$  mV/decade less than 2 h exposure.

was conducted on a freshly polished specimen. The results were consistent and provided conclusive evidence that the OCP deviation was not a result of erroneous measurements. It is difficult to postulate what the exact problem is without a more extensive investigation of the anodic reaction in  $H_2S$  environments, which exceeds the scope of the present paper. It is worth noting that the effect of adsorbed  $OH^-$  on the rate of anodic iron dissolution was not considered in the model.<sup>20</sup> However, whether this is the main cause of

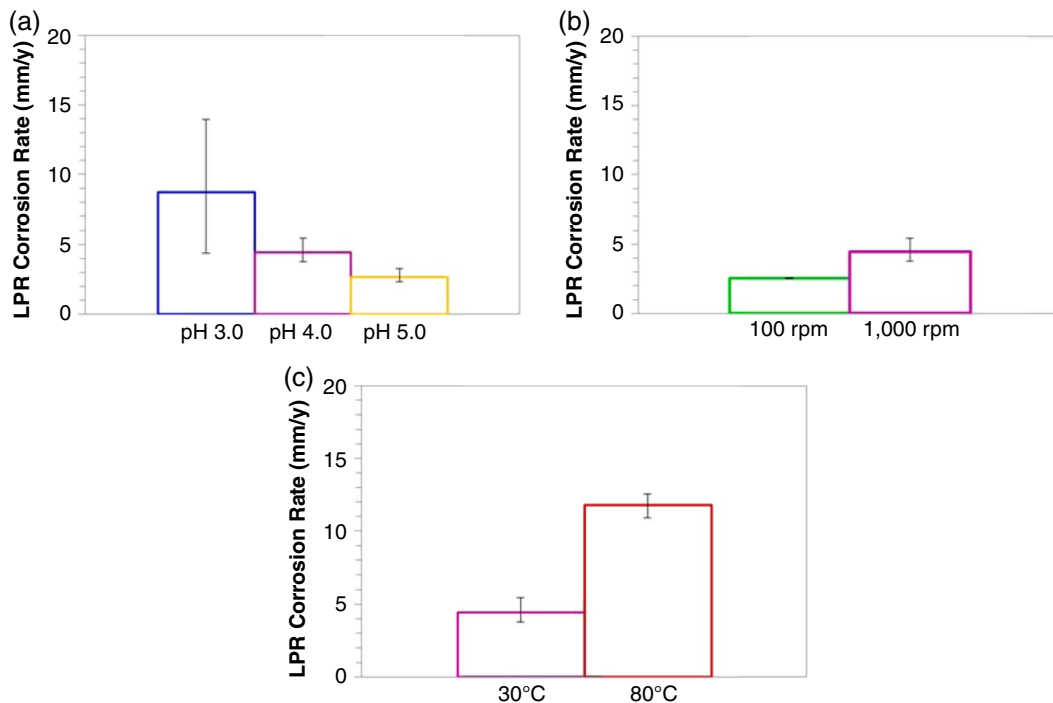


**FIGURE 7.** LPR uniform corrosion rate of X65 in a bulk solution: (a)  $0.096$  MPa  $H_2S$  (960,000 ppm),  $30^\circ C$ , 1,000 rpm; (b)  $0.096$  MPa  $H_2S$ ,  $30^\circ C$ , pH 4.0; and (c)  $0.096$  MPa and  $0.053$  MPa  $H_2S$ , pH 4.0, 3 wt% NaCl, and  $B = 23$  mV/decade less than 2 h exposure.

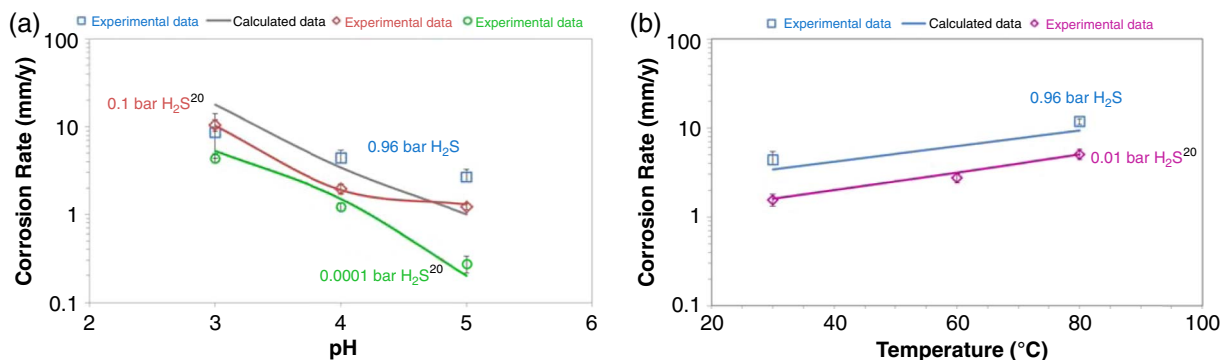


**FIGURE 9.** LPR uniform corrosion rate of X65 in a bulk solution with  $10^{-5}$  MPa  $H_2S$  (100 ppm),  $10^{-2}$  MPa  $H_2S$  (100,000 ppm), and 0.096 MPa  $H_2S$  (960,000 ppm), at 30°C, 1,000 ppm, 3 wt% NaCl, and  $B = 23$  mV/decade less than 2 h exposure.<sup>20</sup>

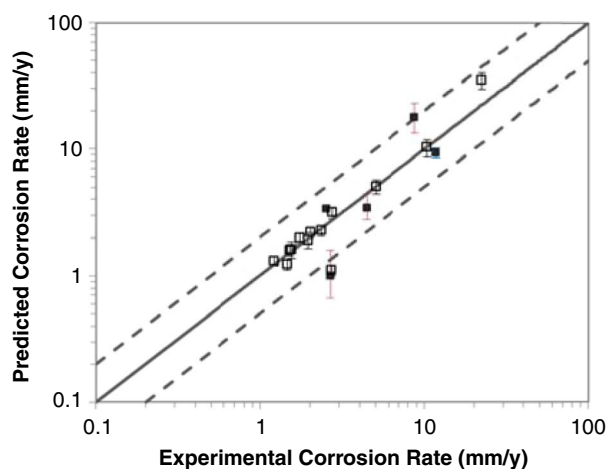


**FIGURE 10.** Parity plot of the predicted uniform corrosion rate using a mechanistic sour corrosion model<sup>20</sup> for short-term exposure of mild steel to  $H_2S$  environments at different conditions in the absence of an iron sulfide layer on the surface vs. measured LPR corrosion rate.

the discrepancy seen at pH 5.0 requires further research.

The performance of the model at lower velocity is shown in Figure 5. This 100 rpm experiment was repeated twice. In this condition, the measured data are in good agreement with the calculated ones, particularly at the lower current densities. At the higher current densities, the discrepancy seen in the cathodic limiting current is a result of the abovementioned hydrogen gas bubble evolution. For the anodic reaction, the deviation is most likely a result of accumulation of ferrous ions at the steel surface at lower rotation speed and formation of an iron sulfide layer, leading to some type of “pre-passivation” behavior.

Data from higher temperature are presented in Figure 6, where the average of data from two potentiodynamic sweeps conducted at 80°C is shown. It is important to mention that the  $pH_2S$  in these experiments was 0.053 MPa because of an increase of the water vapor in the glass cell that was at

atmospheric conditions. Similar to previous conditions, at lower current densities there is a very good agreement between measured and calculated data, while the discrepancies at higher current densities are present for the same reasons as described above.

LPR measurements were conducted in each experiment to measure the uniform corrosion rate, and the results are summarized in Figure 7. The bars are the average of the measured corrosion rate values from repeated experiments, and the error bars show the maximum and minimum deviation from the average. As would be expected, the bare steel corrosion rate decreased with pH, and increased with velocity and temperature. Figure 8 summarizes the uniform corrosion rate of the X65 specimen at different pH values and  $H_2S$  partial pressures. The data at  $10^{-5}$  MPa and  $10^{-2}$  MPa  $H_2S$  were previously reported by Zheng, et al.<sup>20</sup> Figure 9 shows the calculated and measured uniform corrosion rate at different pH values and temperatures. The experimental data at 0.096 MPa  $H_2S$  show some deviations at pH 3.0 and 5.0; however, at pH 4.0 at different temperatures the calculated data are in good agreement with the measured data. The comparison of calculated and measured uniform corrosion rates is shown in Figure 10 as a parity plot. The open symbols are the original experimental data reported by Zheng, et al.,<sup>20</sup> for lower  $pH_2S$ , which are almost in perfect agreement with the predicted corrosion rate. This is to be expected as the model<sup>20</sup> was developed and calibrated using the same low-pressure data (ranging from  $10^{-7}$  MPa to  $10^{-2}$  MPa  $pH_2S$ ). The bold squares in Figure 10 are the results from the current study, conducted at approximately 0.1 MPa  $pH_2S$ , and are also in good agreements with the model calculations. This is of importance as the current data were obtained in an independent study conducted at a much higher  $pH_2S$ .

The current study confirmed that the physico-chemical processes underlying  $H_2S$  corrosion in the absence of protective iron sulfides are very similar across a wide range of  $pH_2S$ . It also demonstrated that the abovementioned mechanistic corrosion model is valid across a broad range of  $pH_2S$  conditions.

## CONCLUSIONS

- ❖ There is a lack of reliable, systematically collected, coherent corrosion data from experiments conducted at high pH<sub>2</sub>S based on sound electrochemical measurements. The present study was conducted to close this gap.
- ❖ It was found that the physicochemical processes underlying H<sub>2</sub>S corrosion in the absence of protective iron sulfides are very similar across a wide range of pH<sub>2</sub>S.
- ❖ The existence of the so-called “double wave” in the cathodic sweeps arises from the two independent cathodic reactions: H<sup>+</sup> reduction and direct H<sub>2</sub>S reduction.
- ❖ It was demonstrated that the calculated corrosion rates based on the mechanistic corrosion model of Zheng, et al.,<sup>20</sup> are in reasonable agreement with the experimental data for a broad range of H<sub>2</sub>S concentrations (up to 0.1 MPa partial pressure of H<sub>2</sub>S).

## ACKNOWLEDGMENTS

The authors would like to express their appreciation to Dr. Yougui Zheng and Mr. Aria Kahyarian for their contributions to this work. Also, the technical support from the lab's staff at The Institute for Corrosion and Multiphase Technology by Mr. Cody Shafer, Mr. Alexi Barxias, and Mr. Phil Bullington is highly appreciated.

## REFERENCES

1. W.R. Whitney, *Corrosion* 3 (1947): p. 331-340.
2. D.C. Bond, G.A. Marsh, *Corrosion* 6, 22 (1950): p. 22-28.
3. F.H. Meyer, O.L. Riggs, R.L. McGlasson, J.D. Sudbury, *Corrosion* 14 (1957): p. 69-75.
4. P.H. Tewari, A.B. Campbell, *Can. J. Chem.* 57 (1979): p. 188-196.
5. D.E. Milliams, C.J. Kroese, *Internal External Protection Pipes* (1979): p. 205-214.
6. J.B. Sardisco, R.E. Pitts, *Corrosion* 21 (1965): p. 350-354.
7. J.B. Sardisco, R.E. Pitts, *Corrosion* 21 (1965): p. 245-253.
8. A. Dravnieks, C.H. Samans, *J. Electrochem. Soc.* 105 (1958): p. 183-191.
9. E.C. Greco, W.B. Wright, *Corrosion* 18 (1962): p. 119-124.
10. W.F. Rogers, J.A. Rowe, “Corrosion Effects of Hydrogen Sulfide and Carbon Dioxide in Oil Production,” Proc. Fourth World Petroleum Congress (London, United Kingdom: WPC, 1955), p. 479-499.
11. S.N. Smith, M.W. Joosten, “Corrosion of Carbon Steel by H<sub>2</sub>S in CO<sub>2</sub> Containing Oilfield Environments,” CORROSION 2006, paper no. 115 (Houston, TX: NACE International, 2005).
12. P.W. Bolmer, *Corrosion* 21 (1965): p. 69-75.
13. B. Tribollet, J. Kittel, A. Meroufel, F. Ropital, F. Grosjean, E.M.M. Sutter, *Electrochim. Acta* 124 (2014): p. 46-51.
14. S.P. Ewing, *Corrosion* 11 (1955): p. 497-501.
15. J.B. Sardisco, W.B. Wright, E.C. Greco, *Corrosion* 19 (1963): p. 354-359.
16. D.R. Morris, L.P. Sompaleanu, D.N. Veysey, *J. Electrochem. Soc.* 127 (1980): p. 1228-1235.
17. A. Anderko, P. Mckenzie, R.D. Young, *Corrosion* 57 (2001): p. 202-213.
18. S.N. Smith, “A Proposed Mechanism for Corrosion in Slightly Sour Oil and Gas Production,” Corrosion 1993, paper no. 1304 (Houston, TX: NACE, 1993).
19. W. Sun, S. Nešić, *Corrosion* 65 (2009): p. 291-307.
20. Y. Zheng, B. Brown, S. Nešić, *Corrosion* 70 (2014): p. 351-365.
21. D.W. Shoosmith, P. Taylor, M.G. Bailey, D.G. Owen, *J. Electrochem. Soc.* 127 (1980): p. 1007-1015.
22. L.G. Benning, R.T. Wilkin, H. Barnes, *Chem. Geol.* 167 (2000): p. 25-51.
23. W.H. Thomason, “Formation Rates of Protective Iron Sulfide Films on Mild Steel in H<sub>2</sub>S-Saturated Brine as a Function of Temperature,” CORROSION 1978, paper no. 41 (Houston, TX: NACE, 1978).
24. I.H. Omar, Y. Gunaltun, J. Kvarekval, A. Dugstad, “H<sub>2</sub>S Corrosion of Carbon Steel Under Simulated Kashagan Field Conditions,” CORROSION 2005, paper no. 300 (Houston, TX: NACE, 2005).
25. Y. Zheng, J. Ning, B. Brown, S. Nešić, *Corrosion* 71 (2015): p. 316-325.
26. K.J. Lee, “A Mechanistic Modeling of CO<sub>2</sub> Corrosion of Mild Steel in the Presence of H<sub>2</sub>S” (Ph.D. diss., Ohio University, 2004).
27. J. Kvarekval, A. Dugstad, “Pitting Corrosion in CO<sub>2</sub>/H<sub>2</sub>S-Containing Glycol Solutions Under Flowing Conditions,” CORROSION 2005, paper no. 631 (Houston, TX: NACE, 2005).
28. D. Abayarathna, “The Effect of Surface Films on Corrosion of Carbon Steel in a CO<sub>2</sub>-H<sub>2</sub>S-H<sub>2</sub>O System,” CORROSION 2005, paper no. 624 (Houston, TX: NACE, 2005).
29. M. Liu, J. Wang, W. Ke, E.-H. Han, *J. Mater. Sci. Technol.* 30 (2014): p. 504-510.
30. S. Nešić, “Carbon Dioxide Corrosion of Mild Steel,” in *Uhlig's Corrosion Handbook*, ed. R.W. Revie (Hoboken, NJ: John Wiley & Sons, Inc., 2011): p. 229-245.
31. M. Eisenberg, C.W. Tobias, C.R. Wilke, *J. Electrochem. Soc.* 101, 6 (1954): p. 306-320.
32. M. Nordsveen, S. Nešić, R. Nyborg, A. Stangeland, *Corrosion* 59 (2003): p. 443-456.
33. J.O. Bockris, D. Drazic, A.R. Despic, *Electrochim. Acta* 4, 2-4 (1961): p. 325-361.
34. O.M. Suleimenov, R.E. Krupp, *Geochim. Cosmochim. Acta* 58 (1994): p. 2433-2444.
35. S. Nešić, J. Postlethwaite, S. Olsen, *Corrosion* 52 (1996): p. 280-294.
36. H. Ma, X. Cheng, G. Li, S. Chen, *Corros. Sci.* 42 (2000): p. 1669-1683.
37. O.M. Suleimenov, T.M. Seward, *Geochim. Cosmochim. Acta* 61 (1997): p. 5187-5198.
38. A. Kahyarian, B. Bruce, S. Nešić, *Corrosion* 72, 12 (2016): p. 1539-1546.

## NOMENCLATURE

$\alpha_c$	Transfer coefficient of electrochemical reaction (-)
b	Tafel slope (V)
$c_i$	Concentration of species i in the bulk (mol/m <sup>3</sup> )
$c_{i,ref}$	Concentration of species i in the bulk at reference conditions (mol/m <sup>3</sup> )
$D_i$	Diffusion coefficient of species i (m <sup>2</sup> /s)
$D_{i,ref}$	Reference diffusion coefficient of species i at reference conditions (m <sup>2</sup> /s)
$d_{RCE}$	RCE diameter (m)
$\rho$	Iron density (kg/m <sup>3</sup> )
$\Delta H$	Enthalpy of activation (J/mol)
$E_{corr}$	Electrode corrosion potential (V)
$E_{rev(H^+)}$	Reversible potential (V)
F	Faraday's constant (C/mol)
$i_c$	Current density (A/m <sup>2</sup> )
$i_{\alpha}$	Charge transfer current density (A/m <sup>2</sup> )
$i_j^d$	Mass transfer limiting current density for reaction j (A/m <sup>2</sup> )
$i_j^0$	Exchange current density for reaction j (A/m <sup>2</sup> )
$i_{j,ref}^0$	Exchange current density of reaction j at reference conditions (A/m <sup>2</sup> )
$k_m$	Mass transfer coefficient (m/s)
$k_{sol}$	Henry's constant (mol/bar)

$K_{\text{H}_2\text{S}}$	H <sub>2</sub> S first dissociation constant	Re	Reynolds number (-)
$M_{\text{Fe}}$	Iron molar mass (kg/kmol)	Sc	Schmidt number (-)
$\mu$	Water viscosity (kg/m·s)	Sh	Sherwood number (-)
$\mu_{\text{ref}}$	Water viscosity at reference conditions (kg/m·s)	$T_c$	Temperature (°C)
$P_{\text{H}_2\text{S}}$	H <sub>2</sub> S partial pressure (bar)	$T_{\text{ref}}$	Reference temperature (K)
$P_{\text{H}_2}$	H <sub>2</sub> partial pressure (bar)	$T_K$	Temperature (K)
R	Universal gas constant (J/mol·K)	$\theta_{\text{HS}}$	Surface coverage (-)